Interfacial Structure in Conjugated Polymers: Characterization and Control of the Interface between Poly(9,9-dioctylfluorene) and Poly(9,9-dioctylfluorene-*alt*-benzothiadiazole)

Anthony M. Higgins,*,†,# Simon J. Martin,† Mark Geoghegan,† Sasha Y. Heriot,† Richard L. Thompson,‡ Robert Cubitt,§ Robert M. Dalgliesh,⊥ Ilaria Grizzi,|| and Richard A. L. Jones†

Department of Physics and Astronomy, University of Sheffield, Hicks Building, Hounsfield Road, Sheffield, S3 7RH, U.K., Department of Chemistry, University of Durham, South Road, Durham DH1 3LE, U.K., Institut Laue-Langevin, 6 rue Jules Horowitz, BP 156, F-38042 Grenoble Cedex 9, France, ISIS, Rutherford Appleton Laboratory, Didcot, OX11 0QX, U.K., and Cambridge Display Technology, Greenwich House, Greenwich Rise, Madingley Road, Cambridge, CB3 0TX, U.K.

Received January 11, 2006; Revised Manuscript Received May 8, 2006

ABSTRACT: Specular neutron reflectivity and nuclear reaction analysis (NRA) are used to measure the interfacial width between poly(9,9-dioctylfluorene) (F8) and poly(9,9-dioctylfluorene-*alt*-benzothiadiazole) (F8BT) in a 500 nm bilayer. Annealing at temperatures up to 280 °C allows us to vary this width over a large range, from ∼1 nm to greater than 30 nm. Approximate calculations using the predictions of self-consistent field theory (SCFT) for both Gaussian and semiflexible chains suggest that in the liquid−liquid regime the Gaussian results of SCFT are valid for this system. We also demonstrate the ability to control the interfacial width in 100 nm bilayers, on both silicon and indium tin oxide (ITO). The procedure of "preannealing" the F8 and F8BT layers, before bringing them together to make a bilayer, allows us to independently control the interfacial width and the properties of the bulk of these 100 nm films.

Introduction

It is well established that the performance of photovoltaic cells and light emitting diodes (LEDs) fabricated from conjugated polymers can be greatly affected by morphology. For instance, binary polymer blend devices, with the same overall blend ratio but different processing conditions, can exhibit considerable differences in efficiency.[1,2] Pairs of polyfluorene-based polymers can be used in the form of either blends[1−4] or bilayers[5−7] to make either photovoltaic cells[1,5] or LEDs.[2,4,6] The advantage of the bicontinuous morphology found in phase-separated blends, is that this provides a large interfacial area that is likely to be beneficial to the operation of a photovoltaic cell. The optimum morphology for a photovoltaic cell is determined by a balance between exciton dissociation (which requires lots of interface) and charge transport (which benefits from a simple conduction path from the interface to the electrodes).[1,8] In an LED, good performance is determined by both balanced charge injection/transport from the electrodes to the polymer/polymer interface and efficient recombination at this interface. A recent study of polyfluorene-based LEDs found that devices with a predominantly stratified morphology can exhibit greater efficiency than laterally phase-separated blends with the same average composition.[2] The simplest form of stratified blend morphology is the bilayer, which can be formed by either direct spin-coating or by floating one polymer film onto the surface of water and then depositing it onto the other polymer. Bilayers hold the advantage of having a much better characterized morphology than thin-film blends. To date, the well-controlled architectures of polyfluorene-based bilayers have enabled quantitative comparison between modeling and experiment in photovoltaic cells[5] and studies of the effect of electric field strength on charge recombination in LEDs.[6]

The nature of the polymer−polymer interfaces within both blends and bilayers is of great importance for device performance, as it is here that either charge recombination or exciton dissociation occurs. However, in common with other polymeric interfaces, conjugated polymer interfaces are not molecularly sharp. Even bilayers prepared by a film floating process will have an interfacial width of around 1 nm, and this can be increased further by thermal processing.[9] Conjugated polymers also have much larger chain rigidity than amorphous, flexible polymers such as polystyrene and poly(methyl methacrylate) (PMMA), which have been the focus of many interfacial studies to date.[10−12] Theoretical studies and simulations predict this to be a crucial factor in the degree of molecular intermixing at polymer−polymer interfaces.[13,14]

In this paper we look at the interface between two polyfluorene-based polymers; poly(9,9-dioctylfluorene) (F8) and poly(9,9-dioctylfluorene-*alt*-benzothiadiazole) (F8BT). This pair of polymers can be used to make an efficient LED. Spin-coated blends of F8 and F8BT form a complex phase-separated morphology with a large interfacial area between F8-rich and F8BT-rich regions.[15−17] Here we use the technique of film floating to make a bilayer, and then we investigate the effect of annealing on the degree of intermixing at the F8/F8BT interface. Our aim is to see whether this procedure can be used to make bilayers with interfacial widths that can be varied over a wide range. The motivation for this study is as follows: (i) to compare

* Corresponding author. E-mail: a.m.higgins@swansea.ac.uk.
† Department of Physics and Astronomy, University of Sheffield,
‡ Department of Chemistry, University of Durham.
§ Institut Laue-Langevin.
⊥ ISIS, Rutherford Appleton Laboratory.
|| Cambridge Display Technology, Greenwich House.
Present address: Multidisciplinary Nanotechnology Centre, School of Engineering, University of Wales Swansea, Singleton Park, Swansea SA2 8PP, U.K.

10.1021/ma060072w CCC: $33.50
Published on Web 08/16/2006

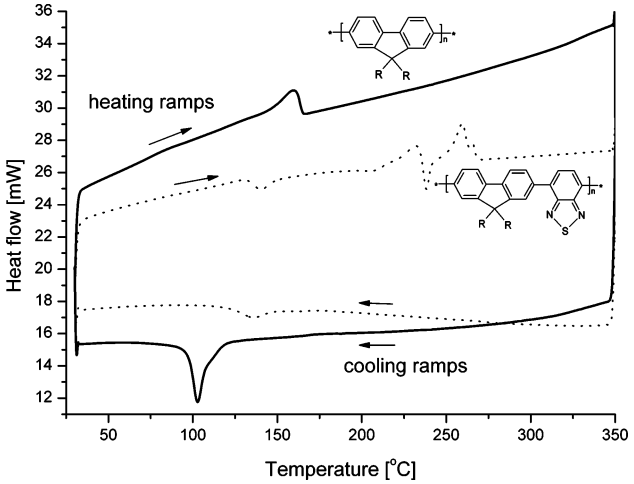

Figure 1. DSC traces for dF8 and F8BT heated/cooled at 20 °C/min. The full line is the data for dF8 and the dotted line is the data for F8BT. The chemical structure of both polymers is also shown. R = C_8H_{17} or C_8D_{17} (see text for details).

the interface between two different conjugated polymers with amorphous, flexible polymers and with existing theories for the interfacial behavior of semiflexible polymers and (ii) to establish a methodology for fabricating well-controlled interfaces, which can be used to study the effect of interfacial properties on device performance. We do not expect that bilayers themselves will necessarily provide a route to increased efficiency of LEDs (although this possibility is certainly worthy of further investigation, especially given recent findings[2]), but they provide a means of varying polymer/polymer interfaces in a well-controlled manner, which we hope will contribute to a clearer understanding of the effects of interface structure on charge recombination and hence device performance. The paper is organized as follows: Following the description of the experimental procedures, the results and discussion section is split into three areas beginning with measurements on ~500 nm bilayers. These measurements will then be compared with theoretical predictions for Gaussian and semiflexible polymer chains. Finally, we discuss work on ~100 nm bilayers, where we present a methodology for LED fabrication that has the potential to provide a direct comparison between interfacial width and device performance.

Experimental Section

Polymer Synthesis and Characterization. The conjugated polymers were supplied by CDT Ltd, Cambridge, U.K. The F8BT has a weight-average molecular weight (M_w) of 197 000 g mol^{-1} and a number-average molecular weight (M_n) of 101 000 g mol^{-1}. A partially deuterated version of poly(9,9-dioctylfluorene) (dF8) was also supplied, with the octyl side chains on alternate monomers being fully deuterated (this was enabled by the Suzuki coupling mechanism that was used to synthesize all of the polymers[18]). This partial deuteration gives sufficient contrast to enable the properties of buried dF8/F8BT interfaces to be probed. The dF8 has M_w = 545 200 g mol^{-1}.and M_n = 145 000 g mol^{-1}. All molecular weights quoted above are from gel permeation chromatography (GPC) referenced to polystyrene standards. The F8BT monomer has a molecular weight of 522 g mol^{-1} and the dF8 monomer has a molecular weight of 388 g mol^{-1}. Membrane osmometry measurements give a degree of polymerization of ~70 for the F8BT and ~140 for the dF8. Figure 1 shows the differential scanning calorimetry (DSC) traces for these two polymer batches. The melting peak (crystalline−nematic transition) for dF8 is visible at around 160 °C. A clear change in gradient, indicative of a glass transition, is also seen at around 80 °C (a similar slope change at slightly lower temperature was seen by previous workers using lower molecular weight F8[19]).The picture for the F8BT is more complicated with melting peaks in the range 210−260 °C and a glass transition temperature (T_g) that is difficult to observe due to recrystallization during the heating ramp. More careful analysis of different F8BT samples, using DSC, dynamic mechanical thermal analysis and thin film interferometry, suggests that the glass transition lies in the range 110 to 130 °C depending on molecular weight and processing history.[20]

Sample Preparation and Annealing. Thick dF8/F8BT bilayer samples were fabricated on silicon blocks (2 in. diameter, 4 mm thickness, with the native oxide layer intact) by directly spin-coating the bottom polymer layer (F8BT) onto the silicon from toluene solution (the silicon substrates were centered on the axis of rotation of the spin-coater). The upper (dF8) layer was spin-coated first onto a piece of freshly cleaved mica before being floated off onto the surface of a bath of deionized water and then deposited onto the silicon/bottom layer to make a bilayer. Thick films were made using 2% solutions (by mass) of dF8 and 3% solutions of F8BT spin-coated at 2000 and 1800 rpm respectively. This gave dF8 layers of mean thickness 221 ± 7 nm and F8BT layers of mean thickness 339 ± 17 nm. Thinner bilayers were prepared on silicon, indium tin oxide (ITO), and mica substrates using 1% dF8 solution spin-coated at 3800 rpm and 1% F8BT solution spin-coated at 1900 rpm, which resulted in dF8 layers of mean thickness 52 nm ± 1 nm and F8BT layers of mean thickness 57 ± 2 nm. For the thinner bilayers inverted samples were also made, in which the dF8 was spin-coated onto ITO and the F8BT floated on top (same concentration solutions and spin speeds). Samples were annealed using two different methods. (i) At temperatures below 200 °C samples were heated in a vacuum oven where the pressure was ~10^{-3} Torr. The samples were placed directly on a machined metal surface within the oven. After 3 h the samples were quenched onto a metal plate at room temperature. The sample temperature was calibrated by attaching a thermocouple to the surface of a test silicon block. This also enabled measurement of the quench rate, which was in excess of 100 °C/min, ensuring that no crystallization of the polymers occurs during the quench.[19] All of the data shown in this paper for annealing temperatures below 200 °C are for samples annealed in a vacuum, in the dark, for 3 h. Neutron reflectivity data for several samples annealed for much longer times (up to 24 h) were very similar to those annealed for 3 h. (ii) At temperatures above 200 °C samples were heated in the dark for only 15 min, on a specially built heater plate within a vacuum chamber, at pressures of ~10^{-6} Torr. These samples were quenched onto a room temperature metal block within the vacuum chamber using a specially designed mechanical arm. Good thermal contact was achieved by using a thin film of low melting point metal (a mixture of indium and bismuth) between the heater and the silicon sample. The chemical purity of the samples was checked after annealing using X-ray photoelectron spectroscopy and Rutherford backscattering. No indium or bismuth was found in the polymer bilayers. Again, a thermocouple in contact with the surface of a test block was used to calibrate the temperature during annealing and confirm that the quench was sufficiently rapid to avoid crystallization. The reason for these different procedures at higher temperatures was to avoid the possibility of degrading the polymers. Both procedures were tested against this possibility, by annealing F8-only films on the same 2 in. silicon blocks and looking at the photoluminescence spectroscopy. No broad peak, characteristic of oxidized F8,[21] was observed for any of the samples. At 280 °C samples were also annealed for times shorter than 15 min (6 and 9 min). The reflectivity curves and fitted interfacial roughnesses of these samples were very similar to the samples annealed for 15 min, confirming that this is sufficient time to establish thermodynamic equilibrium at this temperature.

"Preannealed" samples were also fabricated. Here the dF8 and F8BT layers were annealed separately, before being brought together to make a bilayer. The bottom polymer layer was annealed on a silicon or ITO substrate and the top layer was annealed on cleaved mica.

Sample Measurements. Specular neutron reflectivity measurements were performed at the reflectometers D17 (Institut Laue-Langevin, Grenoble, France) and CRISP (ISIS, Rutherford Appleton Laboratory, U.K.). A comprehensive description of the technique is given by Russell.[22] Both reflectometers use a white beam of neutrons with a time-of-flight detection system. Two or three different incident angles were used to obtain a full reflectivity curve (the reflectivity as a function of momentum transfer perpendicular to the sample plane q_z). At CRISP a q_z-independent resolution of $\sim$ 4% was used, and at D17 we used a setup that gave a resolution varying from $\sim$2.5% at $q_z = 0.01$ Å^{-1} to $\sim$4.5% at $q_z = 0.2$ Å^{-1}.

The ion beam method of ^{3}He nuclear reaction analysis (NRA) can also be used to quantify the width of the interface between a deuterated polymer layer and a protonated polymer layer.[23] We performed such measurements on samples containing very broad interfaces at the ion beam facility at Durham University.[4,24,25] With this technique, a monoenergetic beam of $^3He^+$ ions is incident on the film. On impact with the film, the remaining electron is stripped from the ion, and the nucleus propagates through the sample, losing energy through electronic collisions. In the presence of deuterium, the nucleus may undergo a nuclear reaction, producing a proton and an α particle, either of which may be detected. In these experiments we detect the protons. The energy of the proton is dependent upon the energy of the $^3He^{2+}$ ion at the point at which the reaction occurs, which in turn is dependent on its depth in the sample. The efficiency of retardation of $^3He^{2+}$ ions in a variety of matrix materials is tabulated, and so it is a routine procedure to calculate the depth at which the reaction took place. In this way a volume fraction−depth profile for any deuterated material in a given matrix may be obtained. NRA has a poorer resolution than neutron reflectivity, but it does have the advantage of giving a direct real-space measure of the deuterium depth profile. In our experiments we used a beam energy of 1 MeV and an incident angle between the beam and the sample normal of 75°. The effect of beam damage was reduced by minimizing the total number of ions incident on any one area of the sample. Good statistics were obtained by focusing the beam on several different areas of the sample. The data shown are for the *same samples* on which the reflectivity measurements were made (reflectivity was performed first because of the potential for sample damage in the ion beam).

Results and Discussion

Specular neutron reflectivity measurements were performed on two different types of bilayer. Relatively thick bilayers (>500 nm total thickness) were measured to study how the interfacial width between the dF8 and F8BT layers changed as the samples were annealed at various temperatures spanning the glassy, semicrystalline and nematic liquid crystal phases of both polymers. The root-mean-square (rms) interfacial roughness measured by specular reflectivity is in general composed of two contributions. First there is a molecular level mixing at the interface giving rise to an "intrinsic interfacial width", and second there are nonzero wavelength contributions due to capillary waves or crystallite formation at the interface. Capillary wave contributions to the total interfacial width will change with film thickness because the magnitude of the dispersion force, which determines the low wavevector cutoff to the capillary wave spectrum, is a strong function of film thickness.[12] Our reasons for looking at such thick films were 2-fold. First we wanted to look at the interfacial widths in the regime where the effect of dispersion forces was small and independent of film thickness. In addition, we anticipated that the interfaces may be very broad, and so we used thick films to enable us to accurately quantify interfacial width using a simple bilayer model, with a Gaussian roughness at the surface and interface which was small compared to the overall film thickness. (The interfacial profile is described by an error function, i.e., the convolution of a step function with a Gaussian function of the form $G(z) = (2\pi\sigma^2)^{-1/2} \exp(-z^2/2\sigma^2)$, where σ is the rms roughness of the interface, and z is the direction normal to the sample.) We also looked at thinner samples (total thickness $\sim$100 nm) for a very practical reason; this is the thickness of films typically used to fabricate efficient polymer LEDs, including those made from F8 and F8BT. To corroborate the neutron reflectivity results, NRA measurements were also performed on the thick bilayers that had the broadest interfaces.

Thick Bilayers. Neutron Reflectivity. Before measuring the bilayer samples, measurements were also performed on silicon/dF8 and silicon/F8BT samples annealed at the same temperatures as the bilayers and also on a blank silicon sample. The silicon/dF8 samples were fitted well using a single layer model with a Gaussian surface roughness, with the polymer film thickness, scattering length density and surface roughness as fit parameters. In contrast to the findings of previous workers for a similar deuterated polyfluorene-based polymer on an ITO substrate, no evidence was found for a thin layer next to the silicon substrate that had a lower scattering length density than the rest of the film, for single layers of either F8 or F8BT[26] (we were also able to fit $\sim$60 nm dF8 films on ITO reasonably well using a single layer model). The fitted surface roughness values were compared with those from scanning force microscopy (SFM) measurements on the same samples for all temperatures below 200 °C. The rms roughness measured by tapping mode SFM (Veeco Dimension) used tips with characteristic radii of approximately 10 nm and an image size of 10 μm × 10 μm (which is of the order of the coherence length of the neutrons in the plane of the sample[12,27]). The surface roughnesses fitted from reflectivity and from SFM data showed excellent agreement and rose from $\sim$1 nm for samples annealed at 102 °C to $\sim$4 nm for samples annealed at 192 °C. The agreement between roughnesses determined by SFM and reflectivity of single polymer layers enables us to confidently eliminate surface roughness as a fit parameter in the bilayer samples (in fact we do still fit this parameter, but always compare with SFM measurements on the same sample). The fitted values for the scattering length density of dF8 remained constant with annealing temperature, with a mean value of $(3.3 \pm 0.1) \times 10^{-6}$ Å^{-2} (corresponding to a density of $\sim$1 g cm^{-3}). Unlike dF8, fully protonated F8BT layers on silicon produce reflectivity curves where the position of the critical edge is not sensitive to the scattering length density. In this case the scattering length density is fitted (along with the sample thickness) by fixing the surface roughness at the value obtained from SFM. We again see no systematic change with temperature, with a mean value of $(1.1 \pm 0.1) \times 10^{-6}$ Å^{-2} (also corresponding to a density of $\sim$1 g cm^{-3}).

We now turn to the bilayer samples. Figure 2 shows neutron reflectivity data and fits for the dF8/F8BT/silicon bilayer samples annealed at a range of temperatures. The reflectivity data were fitted using a simple bilayer model which was parametrized by Gaussian surface and interface roughnesses. The scattering length density of the dF8 layer was allowed to vary slightly (within $\sim$3−4% of the mean value) between samples, while that of the F8BT was fixed at the mean value. Parts a and b of Figure 2 show the same data, but in Figure 2b there is a smaller q_z range and the curves are shifted for clarity. It is seen in Figure 2a that there is a continual reduction in the reflectivity as the bilayers are heated to higher temperatures, indicating that some kind of roughening is occurring in the samples. This is also apparent from Figure 2b, where it can

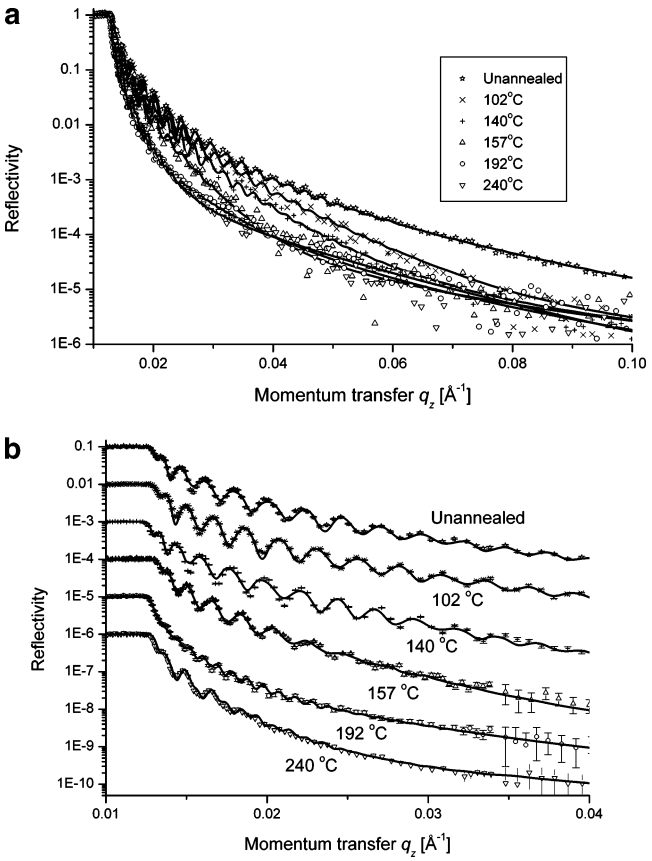

Figure 2. Neutron reflectivity curves and corresponding bilayer fits for thick F8BT/dF8 bilayers on silicon, annealed at the temperatures indicated. The F8BT layers had a mean thickness of 339 nm and the dF8 layers of 221 nm. Figures a and b show the same data sets, with Figure 2b showing the low q_z data only. For clarity, the reflectivity curves are shifted vertically in Figure 2b.

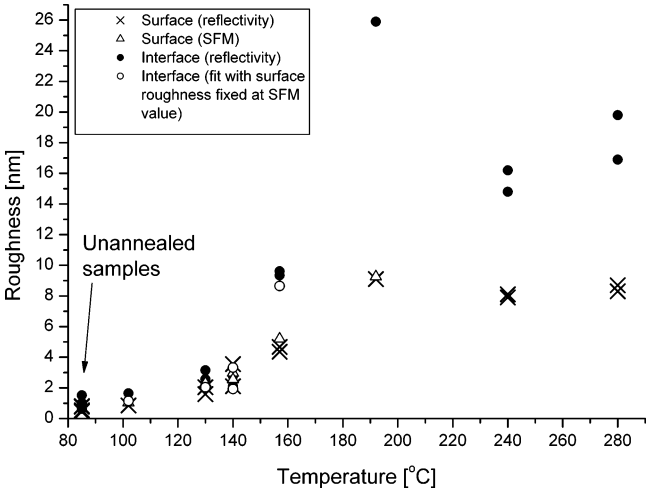

Figure 3. Fitted values of the surface and interfacial roughness of thick F8BT/dF8 bilayers on silicon, as a function of annealing temperature.

clearly be seen that as the temperature rises the fringes become damped more rapidly with q_z. It can be seen from the good quality of the fits in Figure 2b that our use of a simple bilayer model with two fit parameters only is entirely justified. Figure 3 plots the fitted dF8 surface and dF8/F8BT interface roughnesses as a function of annealing temperature, including repeat samples at several temperatures. The first point of note about these data is the size of the interfacial roughness, particularly as the temperature approaches and then exceeds the crystalline/nematic transition temperature of the dF8 (melting peak at ~160 °C). Roughnesses of order 10−20 nm are greatly in excess of what has typically been seen for interfaces between two immiscible amorphous polymers,[10−12] and also for interfaces between conjugated polymer/amorphous polymers.[28] This large increase in roughness as the dF8 melts is readily apparent in Figure 2, when comparing the lower value of the reflectivity and the increased damping of the fringes of the samples annealed at 157 °C and above, with those annealed at lower temperatures. This is particularly dramatic for the sample annealed at 192 °C. Figure 2b shows that the interface has become sufficiently broad in this sample that the fringe spacing is reduced. This is because, unlike all of the other samples, the interface is so broad in this sample that the reflectivity is no longer dominated by interference from neutrons reflected from the top and bottom of the dF8 layer, but from the top and bottom of the entire polymer bilayer. The spacing seen in the reflectivity curve for this sample corresponds to the entire sample thickness of ~540 nm. In fact the interfacial roughness plotted in Figure 3 at 192 °C represents a lower limit on the interfacial roughness. The model reflectivity becomes insensitive to the value of the interfacial roughness once it exceeds ~25 nm (q_z values corresponding to such large roughnesses are found within the region of total reflection). If the interfacial roughness in the bilayer model is allowed to drop much below this value, then one begins to see fringe spacings corresponding to the dF8 layer thickness, that are clearly not present in the data. Also plotted in Figure 3 are the values of the surface roughness for these same samples obtained from SFM measurements (and fits for the interfacial roughness with the surface roughness fixed at the SFM value). Again, these show excellent agreement with the values fitted from the reflectivity data. Note that the change in interfacial roughness with temperature is nonmonotonic, with the sample annealed at 192 °C having a significantly broader interface than those annealed at 240 and 280 °C.

We also annealed some samples at 174 °C. However, these samples produced very poor reflectivity data (very low reflectivity and no fringes evident at all) due to the presence of spherulites covering a significant proportion of the area of the samples (up to 50%). Similar spherulitic structures and very poor reflectivity curves were also obtained when two other samples annealed at 192 °C were measured (the 192 °C sample shown in Figure 2 contained no spherulitic structures). These spherulitic structures are not seen at either of these temperatures in either the single dF8 films or single F8BT films. At 240 °C we also see spherulites, but this time they are isolated structures, covering a very small fraction (≪1%) of the sample area (see Figure 4). Unlike at lower temperatures, at 240 °C spherulites are also seen in the single F8BT films. The reason we only sometimes see spherulites is unknown at present. It appears that there are at least two possible crystal structures for the F8BT films, with the growth rate for each being a complex function of temperature, boundary conditions and also film thickness (see the section on thin bilayers below). The reason that two samples contain many spherulites and one sample contains none at 192 °C may be because the growth rates become comparable and have large temperature dependencies around this temperature. Whether the two crystal structures correlate with the two melting peaks seen in the DSC trace of F8BT is unknown. Previous workers have also seen such spherulitic features in single F8BT films, with the melting peaks in the DSC traces showing significant changes as a function of molecular weight.[29]

One point of note regarding the fitting of the reflectivity curves at 192 °C and above is as follows. While reasonable fits

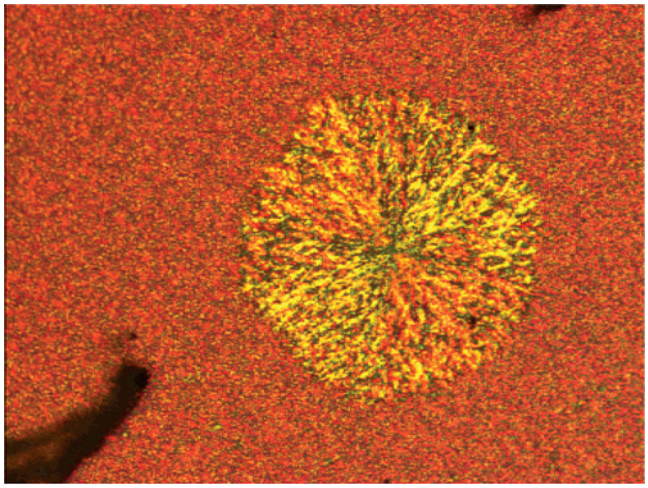

Figure 4. Optical micrograph (using crossed polarizers) of a thick F8BT/dF8 bilayer annealed at 240 °C, showing an isolated spherulite. The image size is 480 μm × 363 μm.

were obtained for these samples with the scattering length density of the F8BT layer set to the mean for F8BT single layers and the native silicon oxide layer thickness and roughness set to the best fit values for the blank silicon sample, it was possible to obtain slightly better fits either by (i) introducing a small (equivalent to ∼1−3 nm of pure dF8) amount of higher refractive index material (i.e., dF8-rich) at the silicon oxide/F8BT interface or (ii) relaxing the constraints on the fit parameters for the oxide layer and the F8BT scattering length density slightly. The former possibility was investigated using NRA, but no evidence for any dF8 at the silicon substrate was found (despite the resolution of the NRA at depth being around 16 nm, the technique was able to detect the presence of ∼3 nm dF8 layers deliberately placed at this depth in test samples). The reason for the required relaxation of the oxide and F8BT constraints (still within physically reasonable bounds) will perhaps become apparent with further measurements of silicon samples, single F8BT films and bilayers.

Thick Bilayers. Nuclear Reaction Analysis. To corroborate the neutron reflectivity results for samples which showed particularly broad interfaces, NRA was performed on the bilayers heated at 192 °C and above. Figure 5 shows the interfacial profiles for these samples plus a sample annealed at 102 °C. The sample annealed at 102 °C (Figure 5a) has an interfacial width that is much narrower than the resolution of the NRA technique. Therefore, the profile in Figure 5a can be used to obtain a value for the resolution of the technique at the depth of ∼200 nm where the interface is located. Using an error function to fit Figure 5a gives us a Gaussian resolution of 16 nm. It is clear from Figure 5b−d that the sample annealed at 192 °C is significantly broader than those annealed at higher temperatures. We can quantify this by fitting the profiles in Figure 5b−d with error functions, and then deconvolving these functions and the resolution function to give the actual interfacial widths of the samples. This process gives us interfacial widths of 34, 20, and 16 nm for annealing temperatures of 192, 240, and 280 °C, respectively. This is in reasonable agreement with the interfacial widths fitted to neutron reflectivity measurements on the same samples (>25, 15, and 17 nm respectively).

Thick Bilayers. Comparison with Theory. Why are the measured interfacial widths for the F8/F8BT system so large compared to those observed for amorphous polymer−polymer interfaces and to previous work on conjugated polymer−amorphous polymer interfaces? We can discount the formation of rough crystalline interfaces accounting for our findings. First we found much smaller roughnesses when we annealed F8/poly(methyl methacrylate) bilayers at similar temperatures, both above and below the melting point of the F8.[28] Second the samples annealed at 280 °C contain very broad interfaces, and this is a liquid−liquid system with both polymers in nematic phases. To understand the behavior of such polymer liquid−liquid systems, we turn our attention to the predictions of self-consistent field theory (SCFT). The intrinsic interfacial width of a polymer A-polymer B interface between two sets of Gaussian chains with identical statistical segment lengths b and a Flory−Huggins interaction parameter χ is given by the Helfand and Tagami result[13] as

$$\omega_I = \frac{b}{(6\chi)^{1/2}} \tag{1}$$

in the limit of high molecular weight ($\chi N \gg 1$, where N is the degree of polymerization). (SCFT gives a composition profile at the interface that varies as $\varphi_A(z) = {}^1/_2[1 + \tanh(z/\omega_I)]$, where $\phi_A(z)$ is the volume fraction of polymer A and z is the position coordinate normal to the interface. This has an almost identical shape to the error function form, with ω_I related to the Gaussian width σ by $\omega_I = (\pi\sigma^2/2)^{1/2}$.[12]) This implies that broad interfaces are due to either large values of b (i.e., relatively stiff polymers) or to low values of χ (i.e., relatively compatible polymers). Conjugated polymers are indeed fairly stiff; F8 having a characteristic ratio C_∞ of 21.5 in tetrahydrofuran (THF)[30] ($C_\infty = b^2/a^2$, where a is the length of the monomer repeat unit). We can use eq 1 to obtain a rough estimate for the lower bound for χ of 0.005 at 280 °C, using the value for C_∞ given above, a = 0.795 nm[30] and the measured Gaussian interfacial width of 17 nm. The reason that this is an estimate of the lower bound for χ is that we have equated the interfacial width measured by neutron reflectivity (or NRA) with the intrinsic interfacial width only. This neglects the contribution of capillary waves in broadening the interface, which may be considerable. However, we think it is reasonable, given the very large interfacial width of ∼17 nm at 280 °C that a significant fraction of this broadening is indeed due to an increased intrinsic width, and that it cannot be entirely accounted for by capillary waves. Indeed a large capillary wave contribution implies that the interfacial tension is low, which in turn implies intrinsic interfacial broadening. We can estimate the size of these two contributions in the Helfand and Tagami case[13] by substituting the SCFT results for the interfacial tension as a function of χ and hence ω_I into the second term of $\omega_{total}^2 = \omega_I^2 + \omega_{capillary\ wave}^2$,[12] where $\omega_{capillary\ wave}$ is the contribution due to the spectrum of capillary waves summed between a low and high wave-vector cutoff (ref 12, eq 7). This can be written as an expression for ω_{total} as a function of ω_I, b, a monomer size and the two capillary wave cutoffs. We perform this calculation for the case of an interface between two thick films, where the low wave-vector cutoff to the measured capillary wave spectrum is set by the in-plane coherence length of the neutrons rather than dispersion forces, and we set the high wave-vector cutoff equal to ω_I. For very large Gaussian widths of around 17 nm this gives a total interfacial width that is dominated by the intrinsic contribution. In this calculation, we have used a neutron coherence length of 20 μm and a monomer size corresponding to a dF8 density of 1 g cm^{-3}, but we find that the dominance of the intrinsic width over the capillary wave contribution is unaffected by large changes to either of these parameters.

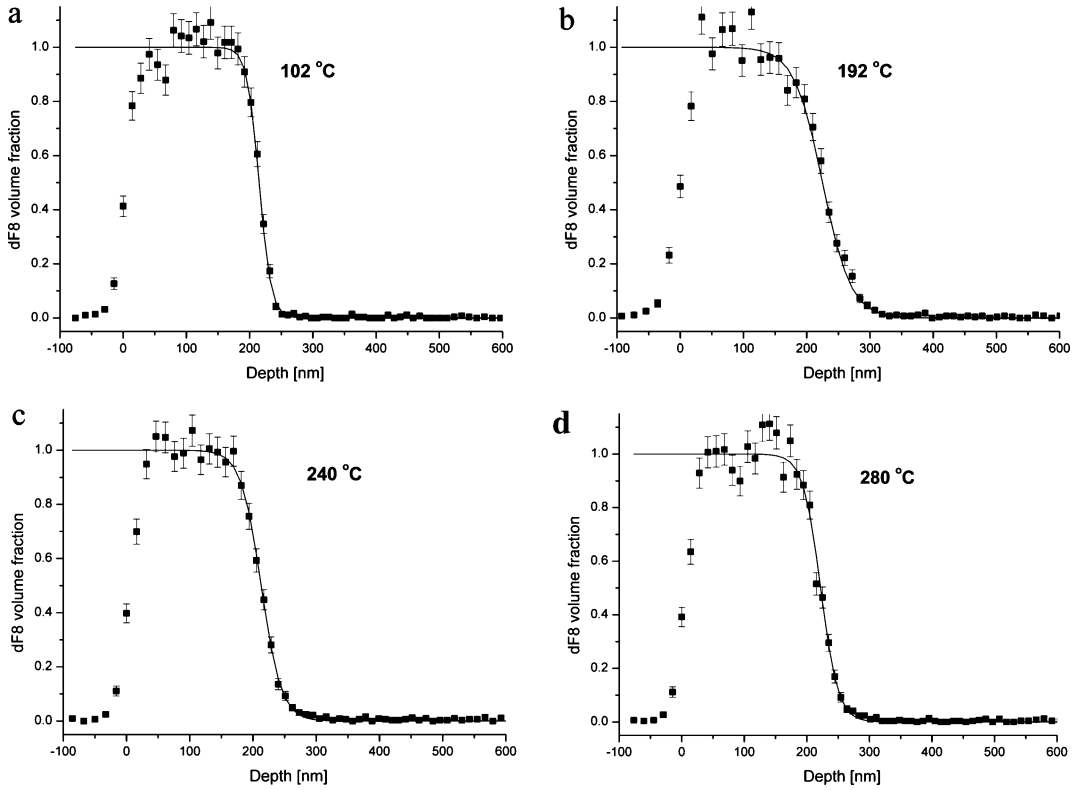

Figure 5. Depth profiles of annealed F8BT/dF8 bilayers obtained using NRA, and corresponding error function fits to the F8BT/dF8 interfacial profiles.

It must be emphasized that eq 1 only gives a rough initial estimate for the lower bound of χ. Our reasons for caution are as follows:

(i) Equation 1 is modified by finite molecular weight (χN of order 1 or lower). Broseta et al. used square gradient theory to calculate that the leading term in the correction is proportional to $1/\chi N$.[31] Tang and Freed then used density functional theory to obtain the following interpolation formula:[32]

$$\omega_I(N) = \frac{b}{(6\chi)^{1/2}}\left[\frac{3}{4}\left(1-\frac{2}{\chi N}\right)+\frac{1}{4}\left(1-\frac{2}{\chi N}\right)^2\right]^{-1/2}; \quad \chi N > 2 \tag{2}$$

The polymers used in these experiments have a relatively low degree of polymerization, and they are also very polydisperse compared to commonly used model polymers such as anionically polymerized polystyrene. To estimate the effect of finite molecular weight we substitute $N \approx 70$ into eq 2, which gives a solution with $\chi = 0.035$. This value of N is that given by membrane osmometry (which measures M_n) of F8BT, and is representative of the lower N polymers found in either layer (largest deviation from eq 1). The higher N polymers are represented by the value of M_w for the dF8. Scaling M_w = 545 200 g mol^{-1} by a factor of 0.39 (which is the scaling factor between M_n found by GPC and membrane osmometry for dF8) gives an estimation for the higher N polymers present in either layer of approximately 530. Substituting $N \approx 530$ into eq 2 gives a value of $\chi = 0.009$. The large polydispersities may also lead to a broader interface than these average molecular weights would imply, due to potential segregation of the lower molecular weight fractions to the interface, driven by their higher entropy of mixing. The extent to which any such molecular weight segregation actually occurs and how this contributes to the large interfacial widths we have observed is unknown at present.

(ii) A potentially even more serious concern is the validity of the SCFT predictions for Gaussian chains in describing the behavior of relatively stiff conjugated polymers. Morse and Frederickson (MF)[14] extended SCFT to study the equilibrium properties of a symmetric interface between two semiflexible polymers, and found qualitative differences compared to the predictions for flexible chains. Their model is parametrized by a statistical segment length b, a monomer length a, a bending modulus of the chains κ ($2\kappa = C_\infty = b^2/a^2$) and a χ parameter (a, b and hence κ are considered to be the same on either side of the interface). In the limit of small chain rigidity ($\kappa\chi \ll 1$) their theory reduces to that for Gaussian chains, with stiffer chains having broader interfaces. Schmid and Muller (SM) also use SCFT for semiflexible chains and find that the intrinsic interfacial width broadens with κ up to at least $\kappa\chi = 2.7$.[33,34] However in the limit of large stiffness ($\kappa\chi \gg 1$) the predicted behavior is completely different. Here MF find two distinct interfacial regions: (a) a narrow region W_1 over which the composition changes from one polymer to the other, in which the polymers are strongly oriented in the plane of the interface, and (b) a broader region W_2 on the order of the persistence length of the polymer, over which the orientational order decays to zero. It is predicted that

$$W_1 \propto \frac{1}{\kappa\chi}\frac{b}{\chi^{1/2}} \tag{3}$$

which is much narrower, by a factor of $1/\kappa\chi$, than for completely flexible chains of the same χ. In summary, it is predicted that at small bending modulus κ, the intrinsic interfacial width will increase with κ up to some maximum value, while at larger values of κ the interfacial width will decrease with κ. (There is a further complication due to potential asymmetry in the bending

modulus which also has an effect on the predictions for Gaussian chains.[35,36] This will not be considered here.)

(iii) One difference between our samples at 280 °C and the predictions of MF and SM is that at 280 °C both polymers are in nematic liquid crystalline phases. In contrast, both MF and SM have isotropic structures for both polymers in the bulk of the films. Despite this, we believe that the predictions of MF and SM are still valid for our experiments. Monte Carlo simulations support the SCFT prediction that there are two distinct interfacial regions, corresponding to compositional and orientational interfacial widths (W_1 and W_2 respectively).[36] As the bending energy of the polymers increases, so does the length scale over which orientational order propagates into the film (W_2). Therefore, for films of finite thickness, the MF and SM predictions imply that the entire film will at some point become effectively nematic as the chain stiffness increases, with the polymer aligned in the plane of the substrate throughout the film (parallel orientation). This will, of course, be affected by any preferential orientation at the substrate/free surface. Recent simulations of nematic liquid crystalline polymer/amorphous polymer interfaces have shown that the far-field boundary condition (homeotropic or parallel) of the liquid crystalline layer can have a significant impact on the interfacial width, with the homeotropic orientation giving broader interfaces.[37] However, evidence suggests that we have a parallel orientation; optical microscopy on single layers of both F8 and F8BT in the nematic phase, and on bilayers annealed at 280 °C shows clear domain structures under crossed polarizers. This orientation has been observed previously for both spin-coated F8 films and aligned F8 films using ellipsometry[38] and X-ray diffraction.[39]

Given these notes of caution we look at the internal consistency of our initial estimation of χ using the predictions for Gaussian chains as follows. We examine a range of χ from the $N \approx 530$ solution to eq 2 to a factor of 3 greater than the $N \approx 70$ solution. (We are being deliberately pessimistic in choosing such a broad range. The higher value of χ represents a fairly extreme situation where the intrinsic width only accounts for 4.5 nm of the total rms roughness of 17 nm, leaving a capillary wave contribution of ~16 nm.) This gives an estimate for the likely range of χ ranging from 0.009 to 0.11, and a range of $\kappa\chi$ from 0.1 to 1.1, which is almost completely within the regime for which MF find agreement with the Helfand and Tagami prediction for Gaussian chains (MF's Figure 2 shows deviation from the Helfand and Tagami prediction for the interfacial tension begins at around $\kappa\chi = 1$). Thus, a Gaussian model of the chains at the interface is internally consistent; the estimated range of χ obtained from the reflectivity data using the Gaussian model gives a range of $\kappa\chi$ where the Gaussian picture remains valid. (The same conclusion is reached if we consider the bending modulus κ for F8BT instead of that for dF8. Although we have no experimental data, we can estimate that the statistical segment length b is smaller for F8BT compared to F8 due to the greater flexibility of the F8BT monomer unit (all C_6 rings in F8 are doubly connected to another C_6 ring, whereas only two-thirds are doubly connected in F8BT). Along with a larger monomer length a for F8BT this suggests that κ for F8BT is smaller than for F8, which would reduce our estimates for the range of $\kappa\chi$, putting us even more firmly in the Gaussian regime.) In contrast, if eq 3 is used to predict χ, this kind of internal consistency does not occur; to obtain such broad interfaces in the regime where eq 3 is valid ($\kappa\chi \gg 1$) would require very *small* values of χ, invalidating the use of this equation. The internal consistency of the Gaussian chain prediction for the interface, raises the interesting possibility that our broad liquid−liquid interfaces could have a structure where the polymers are nematically ordered away from the interface and become more Gaussian as the interface is approached (i.e., exactly the opposite situation to that found by MF for large χN and an isotropic bulk).

Why might roughness growth be nonmonotonic? It is difficult to say with such a limited study of a complex system over a large temperature range. However, it may be of significance that the broadest interface is found for a highly asymmetric system. At 192 °C the dF8 is in the nematic phase, while the F8BT is below its melting point. The temperatures on either side of this show narrower interfaces and have either both polymers below their melting points or both above (in the case of F8BT 240 °C is above one of its two melting peaks and 280 °C is above both of them).

The main practical finding of the study of thick films is that we are able to fabricate F8/F8BT bilayers with interfacial roughness that can be well-controlled over a very large range. However, the interfacial width in both the liquid crystalline and crystalline regimes of both polymers is likely to depend quite strongly on film thickness, as the thickness is reduced and the effect of dispersion forces becomes more important. We now extend the study to the thinner films typically found in working devices.

Thin Bilayers. Neutron Reflectivity. We performed neutron reflectivity measurements on Silicon/F8BT/dF8 bilayers of total thickness ~100 nm which showed roughening of the polymer−polymer interfaces up to ~8−10 nm at 174 °C compared to around 2 nm roughness for annealing temperatures of 130 °C and below (data not shown). We were not able to fit the 174 °C data (we tried two different samples) as well as the samples at lower temperatures, perhaps due to the fact that as the rms roughness becomes a significant fraction of the total film thickness (>5−10%) the simple bilayer model with the assumption of Gaussian interfaces of much smaller width than the film thickness becomes invalid. Potential asymmetry in the interfacial profile is another possibility for the poor fits at 174 °C.[40] The fits also become insensitive to the interfacial roughness once it exceeds around 10 nm. Despite these caveats, it is clear that the roughness at 174 °C is well in excess of 5 nm. An intriguing difference compared to the thicker samples annealed at 174 °C on silicon is that these thin samples show no sign of any spherulitic structures. This may be due to a change in the relative rate of growth of the spherulitic and nonspherulitic crystals as the film thickness changes.

As well as showing the likely range of interfacial widths that one could expect to find within a device made from a phase separated blend of F8 and F8BT, a second reason for looking at thin films is to actually fabricate an LED with a bilayer architecture, and a controllable interfacial width. To get such a device to work would require a transparent anode with an inverted structure (i.e., the F8 on the bottom). To this end we have made such inverted samples on large (2 in. square) ITO substrates (Merck GmbH, Germany). These consist of a macroscopically thick glass substrate with a layer of ITO on top. Neutron reflectivity measurements of such samples, along with inverted samples on silicon substrates, are shown in Figure 6. A blank ITO sample was measured and fitted using a single ITO layer of thickness 124 nm, scattering length density 3.9×10^{-6} Å^{-2}, and rms roughness of 3 nm on top of the glass substrate (this is a very similar scattering length density profile to that reported previously for ITO[26,41]).

In addition to inverted bilayers which have been heated after fabrication, we also made "preannealed" bilayers in which the

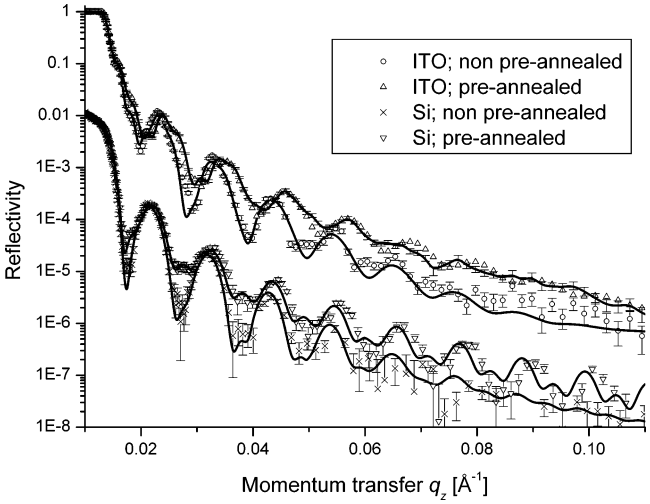

Figure 6. Neutron reflectivity curves and corresponding bilayer fits for thin dF8/F8BT bilayers on ITO and silicon, annealed at 130 °C. For both ITO and silicon substrates the samples were prepared by two different methods, referred to as "preannealed" and "non preannealed" (see text for details). The film thicknesses of the samples was as follows: ITO substrate/non preannealed, dF8, 62 nm, F8BT, ~ 58 nm; ITO substrate/preannealed, dF8, 56 nm, F8BT ~54 nm; silicon substrate/non preannealed, dF8, 53 nm, F8BT ~58 nm; silicon substrate/preannealed, dF8, 55 nm, F8BT, ~56 nm.

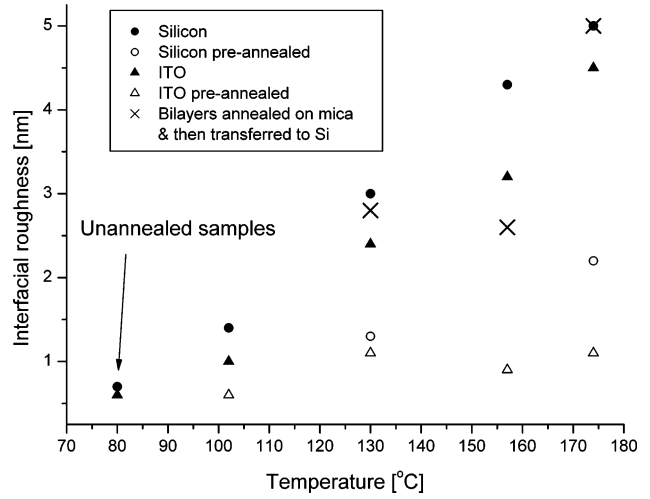

Figure 7. Fitted values of the interfacial roughness of thin F8BT/dF8 bilayers on ITO and silicon, as a function of annealing temperature.

dF8 and F8BT layers were first annealed separately and then brought together to make a bilayer. Annealing obviously affects the material properties of the "bulk" of the films, such as the structure of crystalline and amorphous regions, as well as the interfacial width. The reason for preannealing is therefore to achieve control over the interfacial roughness, independent of the material properties of the bulk of the films. Figure 6 shows that we are indeed able to fabricate two types of bilayer structure, where the films have been annealed at the same temperature but the interfacial roughness can be chosen to be high or low. The fitted values of interfacial roughness in Figure 7 show that we can exercise such control over a broad range of temperatures and hence a broad range of interfacial roughness. Using this approach should allow the fabrication of LEDs which have the same charge transport properties for electrons and holes from the electrodes to the interface and differ only in the width of the polymer−polymer interface. Such a well-characterized architecture could provide a model system for studying how the process of charge recombination within an LED depends on the degree of mixing/interfacial area at the polymer−polymer heterojunction.

We have successfully fabricated bilayer LEDs using both preannealed and non preannealed bilayers of ~100 nm total thickness. However, good performance is only achieved by placing a layer of Baytron (poly(3,4-ethylene dioxythiophene) (PEDT) in the form of a complex with poly(4-styrenesulfonate) (PSS)) at the anode. In such devices, great care is required before direct comparison between device performance and interfacial width can be made, due to the mobility of the PSS component in Baytron. Surface segregation, in which the concentration of PSS is enhanced at the surface, has been found within single Baytron layers,[42,43] with the surface excess changing as the Baytron is heated.[44] The mobility of the PSS within a device would make it difficult to attribute any differences in device performance solely to differences in interfacial width. One way around this is to anneal all F8 layers, F8BT layers and bilayers *before* these are added to the ITO/Baytron substrate. Figure 7 shows three samples where bilayers have been annealed on mica substrates and then floated onto silicon for the purpose of neutron reflectivity measurement. The fitted interfacial roughnesses of these three samples are sufficiently similar to the samples where similar bilayers were annealed on silicon, to indicate that devices with controlled interfacial width can be made by this method.

We expect that similar studies should be possible with other polyfluorene-based pairs to consider the effect of interfacial width on the performance of other LEDs (e.g., based on poly-(9,9′-dioctylfluorene-*alt*-*N*-(4-butylphenyl)diphenylamine) (TFB) and F8BT) and photovoltaic cells. This will be of particular interest because of the formation of interfacial charge-transfer states (exciplexes) which can affect the photoluminescence quenching and hence the efficiency in a photovoltaic cell,[7] and the emission spectra in an LED[45] (exciplexes do not play a significant role in the emission spectra of F8/F8BT blends due to the large differences in the electron affinities of F8 and F8BT which results in rapid Förster transfer of excitons onto the F8BT chain[46]).

Conclusions

We have used neutron reflectivity and NRA to look at the interfacial width between dF8 and F8BT in a 500 nm bilayer. We have shown that thermal processing allows us to vary this width over a large range, from ~1 nm to greater than 30 nm. At annealing temperatures above the melting point of the dF8 (>150 °C), the interfacial width is far greater than observed previously at amorphous polymer interfaces or at amorphous polymer/conjugated polymer interfaces. To understand these broad interfaces we have done some approximate calculations using the predictions of SCFT, for both Gaussian and semi-flexible chains. These calculations suggest that we are in a regime in which the Gaussian results of SCFT are still valid. This procedure is fairly robust, in that a very broad range of values for χ leads to this same conclusion. At present, it is not possible to place a more accurate figure on the value of χ in this system, due to the polydispersity of the polymers and the uncertainties over quantifying the contributions to the total interfacial width from capillary waves and intrinsic molecular level mixing.

We have also demonstrated the ability to control the interfacial width in ~100 nm bilayers on both silicon and ITO. The procedure of "preannealing" the dF8 and F8BT layers allows us to independently control the interfacial width and the properties of the bulk of the films. This opens up the potential

for fabricating LEDs that have identical charge transport properties from the electrodes to the interface, and differ only in the width of the polymer−polymer interface. We believe that this could provide a model system for studying how the process of charge recombination depends on the degree of mixing at polymer−polymer heterojunctions.

Acknowledgment. The authors thank Richard French for designing and building the heater used for annealing/quenching the 2 in. silicon blocks at 240 and 280 °C. We thank David G. Lidzey for the use of his photoluminescence setup, and David G. Lidzey and Monika Voigt for collaborating on the preliminary LED fabrication/measurements. Thanks to Andrew Wildes for help with some of the reflectivity measurements at D17. Finally, A.M.H. thanks Jamie Hobbs in Sheffield and Chris Wright in Swansea for use of their scanning force microscopes. A.M.H. and S.Y.H. acknowledge support from EPSRC (Grant No. GR/R26658/01). S.J.M. acknowledges support from EPSRC platform Grant No. GR/R77544/01.

References and Notes

(1) Arias, A. C.; MacKenzie, J. D.; Stevenson, R.; Halls, J. J. M.; Inbasekaran, M.; Woo, E. P.; Richards, D.; Friend, R. H. *Macromolecules* **2001**, *34*, 6005−6013.
(2) Corcoran, N.; Arias, A. C.; Kim, J. S.; MacKenzie, J. D.; Friend, R. H. *Appl. Phys. Lett.* **2003**, *82*, 299−301.
(3) Halls, J. J. M.; Arias, A. C.; MacKenzie, J. D.; Wu, W.; Inbasekaran, M.; Woo, E. P.; Friend, R. H. *Adv. Mater.* **2000**, *12*, 498−502.
(4) Chappell, J.; Lidzey, D. G.; Jukes, P. C.; Higgins, A. M.; Thompson, R. L.; O'Connor, S.; Grizzi, I.; Fletcher, R.; O'Brien, J.; Geoghegan, M.; Jones, R. A. L. *Nat. Mater.* **2003**, *2*, 616−621.
(5) Ramsdale, C. M.; Barker, J. A.; Arias, A. C.; MacKenzie, J. D.; Friend, R. H.; Greenham, N. C. *J. Appl. Phys.* **2002**, *92*, 4266−4270.
(6) Morteani, A. C.; Ho, P. K. H.; Friend, R. H.; Silva, C. *Appl. Phys. Lett.* **2005**, *86*, 163501.
(7) Dhoot, A. S.; Hogan, J. A.; Morteani, A. C.; Greenham, N. *Appl. Phys. Lett.* **2004**, *85*, 2256−2258.
(8) Arias, A. C.; Corcoran, N.; Banach, M.; Friend, R. H.; MacKenzie, J. D. *Appl. Phys. Lett.* **2002**, *80*, 1695−1697.
(9) Higgins, A. M.; Martin, S. J.; Jukes, P. C.; Geoghegan, M.; Jones, R. A. L.; Langridge, S.; Cubitt, R.; Kirchmeyer, S.; Wehrum, A.; Grizzi, I. *J. Mater. Chem.* **2003**, *13*, 2814−2818.
(10) Fernandez, M. L.; Higgins, J. S.; Penfold, J.; Ward, R. C.; Shackleton, C.; Walsh, D. J. *Polymer* **1988**, *29*, 1923−1928.
(11) Anastasiadis, S. H.; Russell, T. P.; Satija, S. K.; Majkrzak, C. F. *J. Chem. Phys.* **1990**, *92*, 5677−5691.
(12) Sferrazza, M.; Ziao, C.; Jones, R. A. L.; Bucknall, D. G.; Webster, J.; Penfold, J. *Phys. Rev. Lett.* **1997**, *78*, 3693−3696.
(13) Helfand, E.; Tagami, Y. *J. Chem. Phys.* **1972**, *56*, 3592−3601.
(14) Morse, D. C.; Frederickson, G. H. *Phys. Rev. Lett.* **1994**, *73*, 3235−3238.
(15) Wilkinson, C. I.; Lidzey, D. G.; Palilis, L. C.; Fletcher, R. B.; Martin, S. J.; Wang, X. H.; Bradley, D. D. C. *Appl. Phys. Lett.* **2001**, *79*, 171−173.
(16) Morgado, J.; Moons, E.; Friend, R. H.; Cacialli, F. *Adv. Mater.* **2001**, *13*, 810−814.
(17) Morgado, J.; Friend, R. H.; Cacialli, F. *Appl. Phys. Lett.* **2002**, *80*, 2436−2438.
(18) Inbasekaran, M.; Woo, E.; Wu, W.; Bernius, M.; Wujkowski, L. *Synth. Met.* **2000**, *111*−*112*, 397−401.
(19) Grell, M.; Bradley, D. D. C.; Inbasekaran, M.; Woo, E. P. *Adv. Mater.* **1997**, *9*, 798−802.
(20) Caustier, L.; Ph.D. Thesis, University of Cambridge, 2005.
(21) Sims, M.; Bradley, D. D. C.; Ariu, M.; Koeberg, M.; Asimakis, A.; Grell, M.; Lidzey, D. G. *Adv. Funct. Mater.* **2004**, *14*, 765−781.
(22) Russell, T. P. *Mater. Sci. Rep.* **1990**, *5*, 171−271.
(23) Chaturvedi, U. K.; Steiner, U.; Zak, O.; Krausch, G.; Klein, J. *Phys. Rev. Lett.* **1989**, *63*, 616−619.
(24) Geoghegan, M. In *Polymer Surfaces and Interfaces III*; Richards, R. W., Peace, S. K., Eds.; Wiley: New York, 1999; pp 43−73.
(25) Higgins, A. M.; Martin, S. J.; Thompson, R. L.; Chappell, J.; Voigt, M.; Lidzey, D. G.; Jones, R. A. L.; Geoghegan, M. *J. Phys.: Condens. Matter* **2005**, *17*, 1319−1328.
(26) Mitchell, W. J.; Burn, P. L.; Thomas, R. K.; Fragneto, G.; Markham, J. P. J.; Samuel, I. D. W. *J. Appl. Phys.* **2004**, *95*, 2391−2396.
(27) Richardson, R. M.; Webster, J. R. P.; Zarbakhsh, A. *J. Appl. Crystallogr.* **1997**, *30*, 943−947.
(28) Higgins, A. M.; Jukes, P. C.; Martin, S. J.; Geoghegan, M.; Jones, R. A. L.; Cubitt, R. *Appl. Phys. Lett.* **2002**, *81*, 4949−4951.
(29) Banach, M. J.; Friend, R. H.; Sirringhaus, H. *Macromolecules* **2003**, *36*, 2838−2844.
(30) Grell, M.; Bradley, D. D. C.; Long, X.; Chamberlain, T.; Inbasekaran, M.; Woo, E. P.; Soliman, M. *Acta Polym.* **1998**, *49*, 439−444.
(31) Broseta, D.; Fredrickson, G. H.; Helfand, E.; Leibler, L. *Macromolecules* **1990**, *23*, 132−139.
(32) Tang, H.; Freed, K. F. *J. Chem. Phys.* **1991**, *94*, 6307−6322.
(33) Schmid, F.; Muller, M. *Macromolecules* **1995**, *28*, 8639−8645.
(34) Schmid, F. *J. Phys.: Condens. Mattter* **1998**, *10*, 8105−8138.
(35) Helfand, E.; Sapse, A. M. *J. Chem. Phys.* **1975**, *62*, 1327.
(36) Muller, M.; Werner, A. *J. Chem. Phys.* **1997**, *107*, 10764−10776.
(37) Li, X.; Denn, M. M. *Phys. Rev. Lett.* **2001**, *86*, 656−659.
(38) Campoy-Quiles, M.; Etchegoin, P. G.; Bradley, D. D. C. *Phys. Rev. B* **2005**, *72*, 045209.
(39) Kawana, S.; Durrell, M.; Lu, J.; Macdonald, J. E.; Grell, M.; Bradley, D. D. C.; Jukes, P. C.; Jones, R. A. L.; Bennett, S. L. *Polymer* **2002**, *43*, 1907−1913.
(40) Geoghegan, M.; Boue, F.; Bacri, G.; Menelle, A.; Bucknall, D. G. *Eur. Phys. J. B* **1998**, *3*, 83−96.
(41) Martin, S. J.; Jones, R. A. L.; Geoghegan, M.; Higgins, A. M.; Grizzi, I.; Halls, J. J. M.; Kirchmeyer, S.; Dalgliesh, R. M. *Phys. Rev. B* **2005**, *71*, 081308.
(42) Greczynski, G.; Kugler, T.; Salaneck, W. R. *Thin Solid Films* **1999**, *354*, 129−135.
(43) Greczynski, G.; Kugler, T.; Keil, M.; Osikowicz, W.; Fahlman, M.; Salaneck, W. R. *J. Electron Spectrosc. Relat. Phenom.* **2001**, *121*, 1−17.
(44) Jukes, P. C.; Martin, S. J.; Higgins, A. M.; Geoghegan, M.; Jones, R. A. L.; Langridge, S.; Wehrum, A.; Kirchmeyer, S. *Adv. Mater.* **2004**, *16*, 807−811.
(45) Morteani, A. C.; Friend, R. H.; Silva, C. *J. Chem. Phys.* **2005**, *122*, 244906.
(46) Buckley, A. R.; Rahn, M. D.; Hill, J.; Cabanillas-Gonzalez, J.; Fox, A. M.; Bradley, D. D. C. *Chem. Phys. Lett.* **2001**, *339*, 331−336.

MA060072W